Supplementary Material for

Edge Contacts of Graphene formed by Using Controlled Plasma Treatment

Dewu Yue, Chang-Ho Ra, Xiaochi Liu, Daeyeong Lee, and Won Jong Yoo*

SKKU Advanced Institute of Nano-Technology (SAINT), Samsung-SKKU Graphene Center (SSGC), Sungkyunkwan University, 2066, Seobu-ro, Jangan-gu, Suwon, Gyeonggi-do, 440-746 Korea

*Corresponding author, yoowj@skku.edu

Contents:

1. Figure S1-S9.

Figure S1

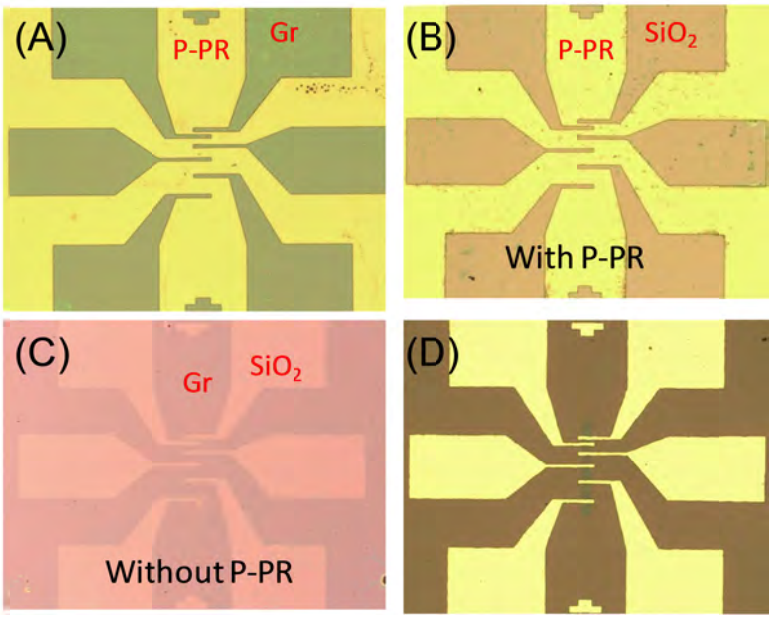

Figure S1. Optical microscopic images of schematic of the pre-plasma fabrication process for the edge-contact. The yellow area indicates that photoresist masked the TLM pattern as well as the other developed area that form the graphene surface. (B) shows the sample after exposure. The pattern without the photoresist is shown in (C). In comparison to that in (A), the graphene was cleanly etched, and the formation of completely edge-contacted graphene was confirmed. (D) shows the final device structure with patterned graphene that was used for the electrical test.

Figure S2

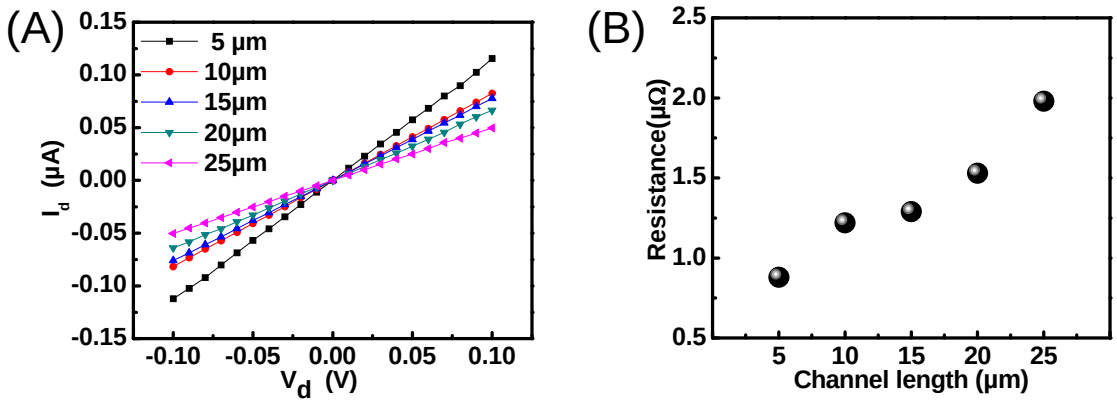

Figure S2. (A) Source-drain current as a function of source-drain voltage. (B) The resistance increasing consistently as the channel length becomes longer.

Figure S3

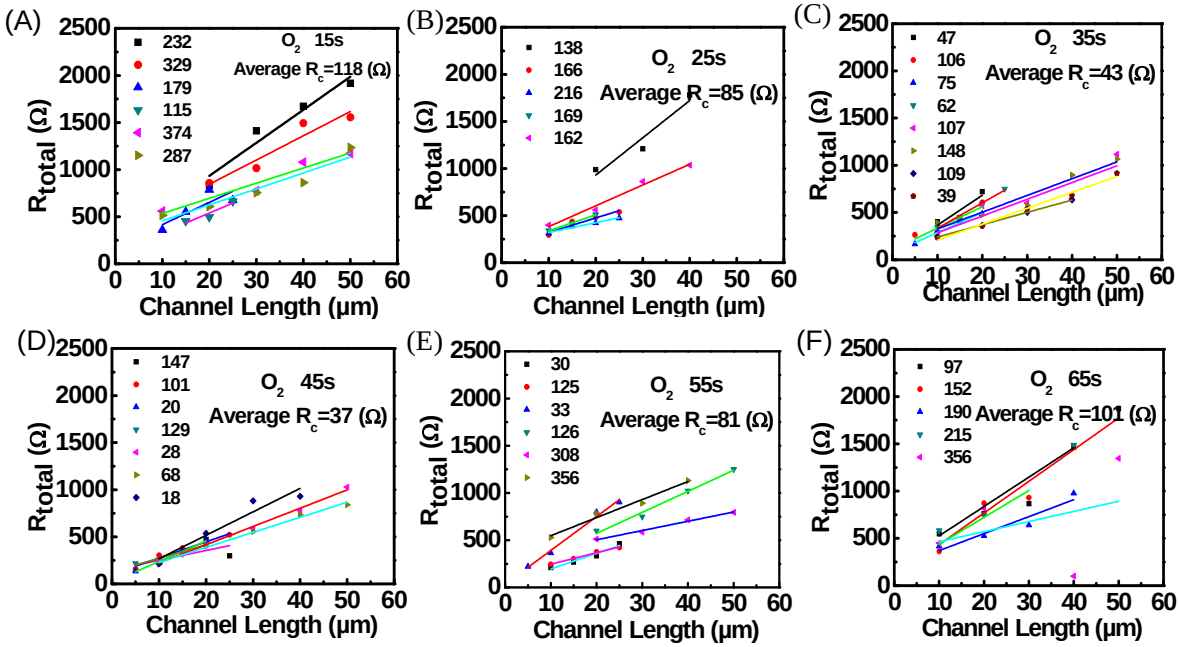

Figure S3. Determination of "edge-contact" contact resistance using the transfer length method (TLM). (A)(B)(C)(D)(E)(F) Deriving contact resistance using the TLM at the gate biases of 0.01 V for six different times of 15, 25, 35, 45, 55, and 65s, respectively.

Figure S4

Processing Time/ Devices Numbers	Range (KΩ·μm)	Average (KΩ·μm)	Maximal Reduction (%)	Average Reduction （%）
5s/4	3.25-8.91	5.19	--	--
15s/6	3.79-5.61	3.80	--	--
25s/5	2.07-3.24	2.55	44	33
35s/8	0.59-2.22	1.31	72	65
45s/7	0.27-2.20	1.10	77	71
55s/6	0.44-5.34	2.45	--	--
65s/5	1.45-5.34	3.03	--	--

Figure S4. A summary of contact resistance metrics comparing the 5, 15, 25, 35, 45, 55, and 65s conditions from 41 sets of devices. 41 sets of FET devices were used to measure the range of R_c, and the lowest average R_c of 1.10 kΩ·μm was obtained from 7 sets of devices with the exposure to oxygen plasma for 45s. The average reduction was estimated by $(R_0 - R_x)/R_0 = \Delta R/R_0$, where $\Delta R/R_0$ represents the reduction seen in the table, R_0 is the constant value of the resistance obtained from exposure to O_2 plasma for 15s which is $R_0 = 3.80\ k\Omega \cdot \mu m$ on average, and R_x is the resistance obtained for different treatment times which is R_x = 2.55, 1.31, 1.10 kΩ·μm on average. In order to obtain results with a higher accuracy, we used a statistical equation to calculate the maximal reduction. For example, the maximal reduction from the 45 s exposure is $77\% = [(\frac{5.61-2.20}{5.61} + \frac{3.79-0.27}{3.79})]/2) \times 100\%$, taking into consideration the entire range of the R_c.

Figure S5

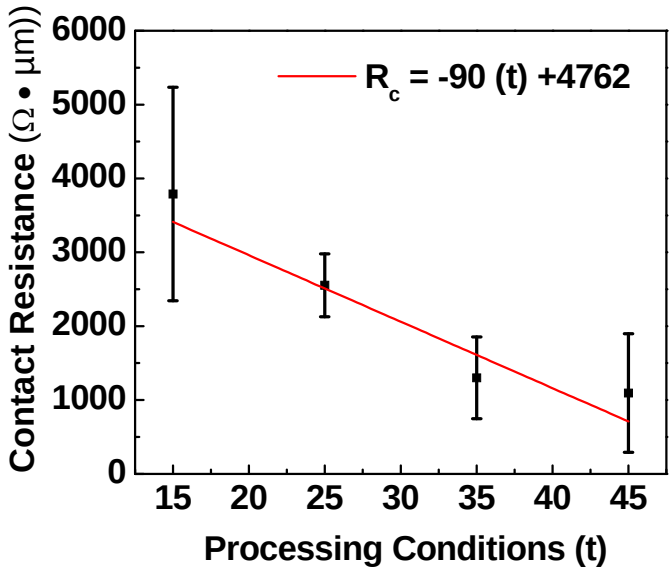

Figure S5. Fitting of the R_c from 15 to 45 s: $R_c(t) = -90t+4762$ [kΩ·μm]

Figure S6

(A)

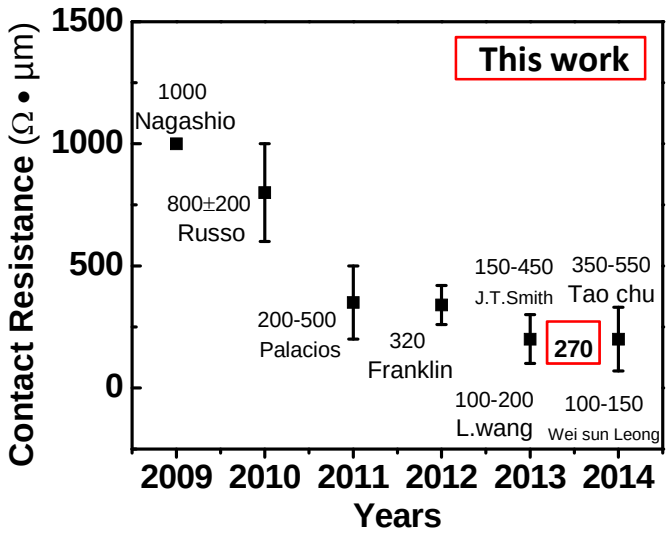

Figure S6. (A) Contact resistance vs years, comparing our results to those obtained in studies performed since 2009 that aimed to reduce the contact resistance. The values of R_c shown in the figure are the lowest in each paper, and more information of these works is shown in Figure S6(B).

Figure S6

(B)

Reference Graphene	Lowest Rc (Ωμm)	Technique to lower Rc
[1]-Exfoliated	1000	Conventional process of surface contact
[2]-Exfoliated	800	Ti-graphene contact in SG, BG and TG.
[3]-Exfoliated	100	BN-Gr-BN structure to form edge contact
[4]-Exfoliated	100	Nickel-Etched-Graphene contacts
[5]-Exfoliated	350	self-aligned edge-contacting scheme
[6]-CVD	320	Double contacts
[7]-CVD	200	Contact area patterning
[8]-CVD	200	Al sacrificial layer

Figure S6 (B) Major contributions[1-8] to reduce contact resistance that we selected since 2009, which makes comparison to our work. Note that the values of R_c shown in the figure are the lowest in each paper.

Figure S7

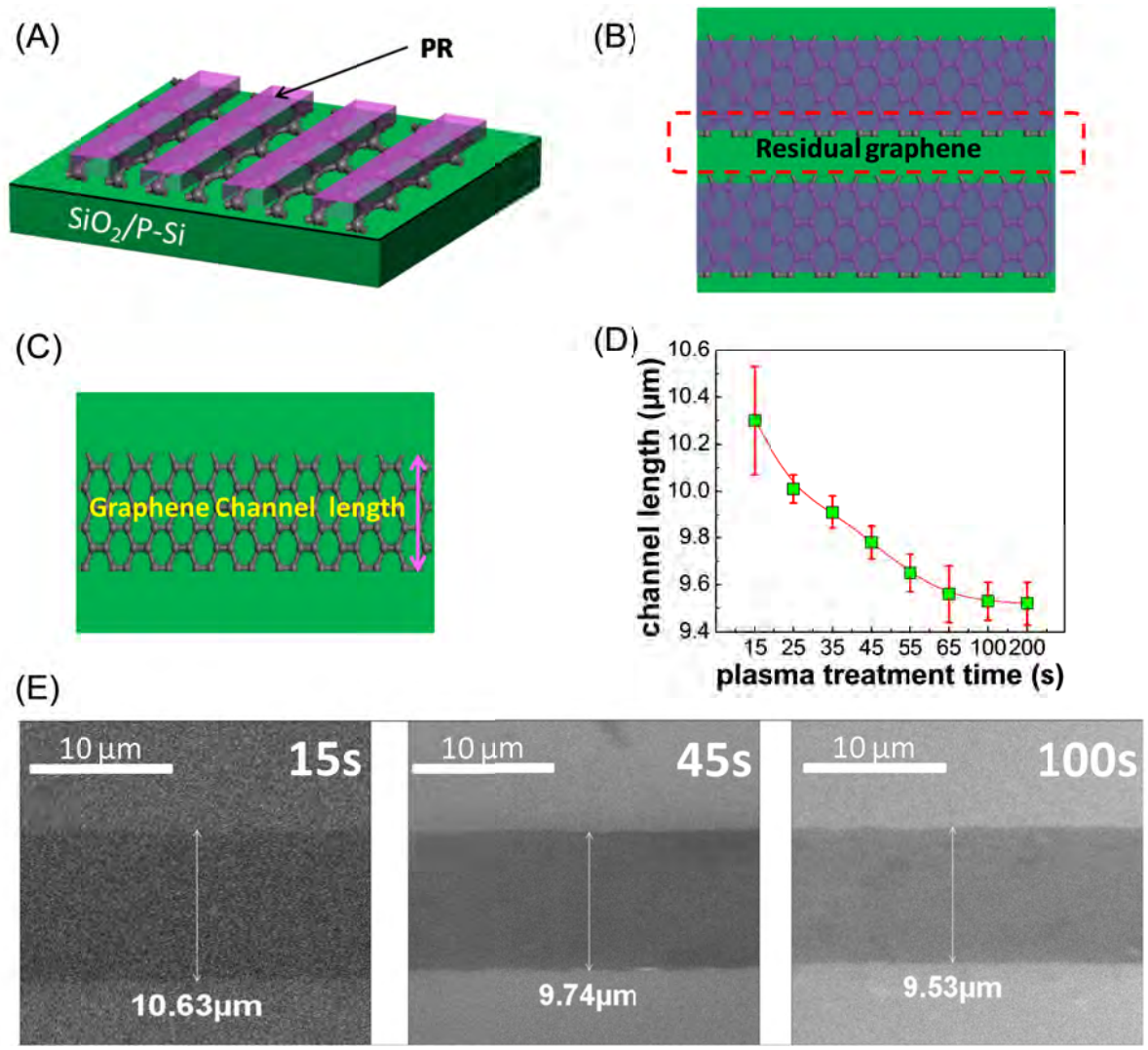

Figure S7. Effects of pre-plasma treatment on the edge structure of patterned CVD-grown graphene. (A) Schematic of the patterned sample. (B) Schematic of the sample after the controlled plasma treatment, showing the residual graphene on the edge of the patterned channel. (C) Schematic illustration of graphene channel after acetone removal. (D) Channel length vs plasma treatment time. (E) SEM images of the graphene films after the treatment by three controlled plasma processing times of 15, 45, and 100s, showing obvious channel length variation.

In order to reveal the changes made on the edge of the graphene, we analyzed how the graphene patterns changed as the plasma treatment time increased. To investigate the effect of the plasma on the structural changes in the edge of the patterned CVD-grown graphene, the same graphene device was designed with four uniformly patterned graphene structures with the same channel length (L) of ~10+0.3 μm. The subsequently deposited metal makes direct contact with the samples, and the actual M-G contact lengths can be controlled with precision by controlling the plasma treatment, as shown in Figure S7(D). A line of best fit for L with respect to the measurements of the edge improvement in the samples treated with plasma for 15 to 45 s can be written as $L(t) = -0.013t+10.34$ [μm] [1] (See Figure S8). Figure S7(E) shows SEM images of graphene films treated with controlled plasma for 15, 45, and 100 s, showing an obvious L variation. [1] can be combined with $R_c(t) = -90t+4762$ [Ω·μm] to obtain the R_c for our system as $Rc(t) = 6923L(t) – 66823$ [Ω·μm] [2]. These equations provide the relation between Rc and the channel length (L) at metal contact edge, and explain quantitatively how contact property is improved by controlled plasma as a function of plasma exposure time**.** When comparing the linear fitting of R_c and channel length shown in Figure S5 and S8 respectively, we found they match more than 95%. So, it supports the structural variation shown in Figure 2(C)-(F). This corroborates our assumption that the controlled plasma treatment can improve the edge structure by facilitating edge-contact.

Figure S8

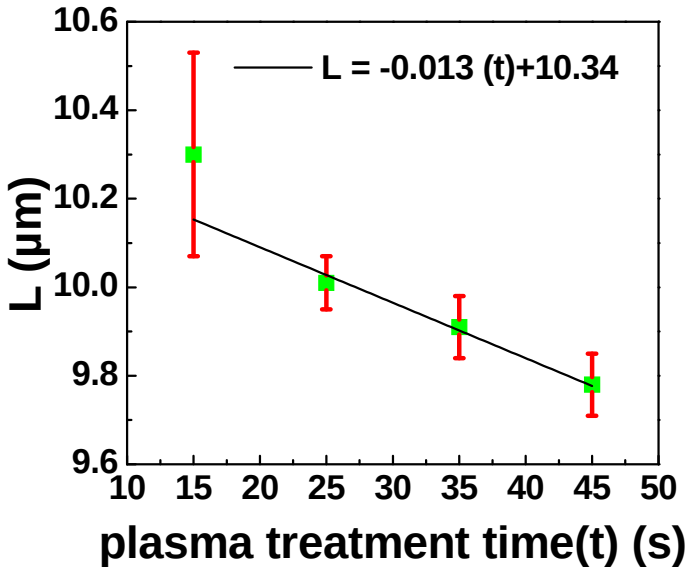

Figure S8 A line of best fit for the channel length (*L*) with respect to the measurements of the edge improvement in the samples treated with plasma for 15 to 45 s: *L(t) = -0.013t+10.34* [μm].

Figure S9

(A)

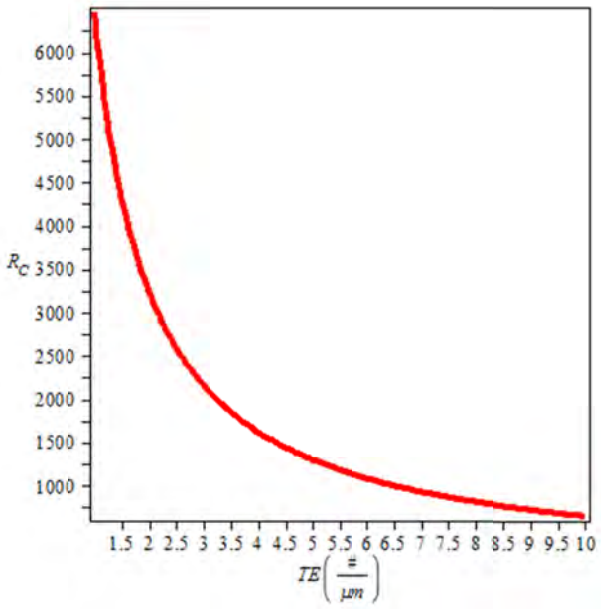

Figure S9 <u>(A)</u> The *ab initio* NEGF transmission efficiency vs. contact resistance (R_c).

Figure S9

(B)

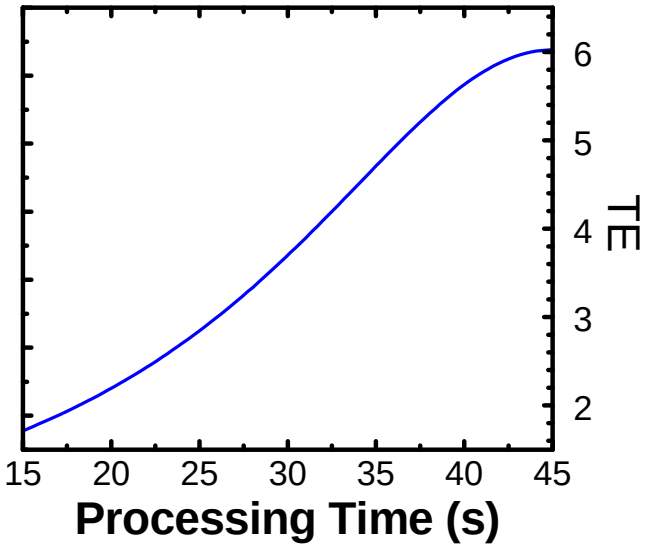

Figure S9 (B) Charge transmission efficiency (TE) as a function of plasma processing time.

2. Enhancement of carrier transport and mobility at the M-G contact junction

Figure S10 shows the transfer characteristics when comparing the plasma durations for 15, 25, 35, 45, 55 and 65 s. An improvement in the current is seen as the plasma treatment time increases. Here, we show a source-drain current via a back-gate voltage with a source-drain voltage ($V_{S\text{-}D}$) of 0.01 V for devices with a channel length (L_{ch}) of 15, 20, and 40 μm. The results indicate that the current is greater at 35, 45, and 55 s**.** Based on mathematical formulas,

$$R_{total} = \rho_{total}(L_{ch} + \Delta L) = \frac{2R_c}{W} + \rho_{ch}L_{ch}\ ,$$

where $\mu = 1/\rho_{total} ne\ and\ \Delta L\ is$ is the additional length involving contacts. Therefore,

$$(L_{ch} + \Delta L)/\mu ne = \frac{2R_c}{W} + \rho_{ch}L_{ch}$$

This explains that increased μ follows the trend of reduced R_c and it is not necessary for the maximum μ to match the minimum R_c,as shown in our results of Figure 2(B) and S10. To confirm the results, we repeated the measurements from the same sample, and the same improvement in the carrier transport was confirmed.

A more thorough theoretical and experimental analysis was performed for the six figure panels shown in Figure S11. First, without taking into account the different channel lengths, all lines in each figure are rather close to each other. For example, Figure S11(a) shows that the source-drain current ($I_{S\text{-}D}$) changes consistently as a function of the back-gate voltage V_b, which demonstrates that the carrier mobility is similar, as shown in the error bars of Figure 2(B), which ranges from 100 – 450 cm^2/Vs. Second, when considering the electrical properties of the devices for the three different channel lengths, the resistance increases as the channel length increases. In the figure for each condition, the currents for L_{ch}=15 μm are all found in the upmost region, in the middle region for L_{ch}=20 μm, and in the downmost region for L_{ch}=40 μm. In addition, the current becomes larger as the treatment time increases from 15 to 55s, indicating an improvement in the carrier transport. Finally, the p-type CVD graphene back-gate-devices can be

clearly analyzed in the six panels. Normally the p and n branches always show moderate asymmetry, and R_c in the p branch is always smaller than that in the n branch[9].

The average mobilities for the devices with six different treatment times are shown in Figure S10. The mobilities were obtained according to

$$\mu = (1/C_{ox}) \times (d\, I_D/d\, V_{BG}) \times (L_{ch}/W_{ch})/V_{S-D}$$

where C_{ox}=1.15×10^{-8}F/cm^2 for 300 nm SiO_2 and $V_{S\text{-}D}$=0.01 V. The exposure to O_2 for 5 – 45s increased the mobility from 299 to 568 cm^2/Vs, as seen in the Figure S10, but the mobility was reduced to 290 cm^2/Vs after 65 s of exposure to O_2 plasma due to over-etching. Short-range scattering due to the intrinsic defects or the dislocations in the CVD graphene is largely the cause for which mobility decreases, limiting the mobility < 1000 cm^2/Vs[8].

The reason for the μ improvement of less than R_c is that the improvement in the contacts is more clearly observed due to doping effect in graphene by gate modulation when the graphene is biased far from the Dirac point. Meanwhile, when V_g sweeps close to the Dirac Point, the resistance in the graphene channel becomes dominant, and a more dramatic change in the current takes place, as seen in our previous work[10]. These findings are also consistent with those reported in other works. Furthermore, the mobility around the Dirac point is generally much higher than that far from the point[1,7]. Despite all of the considerations of the above, the lowest R_c of the CVD-graphene FET devices was obtained from the pre-plasma process of an exposure time of 45 s to O_2, where carrier transport between the G-M interface may have been improved.

Figure S10

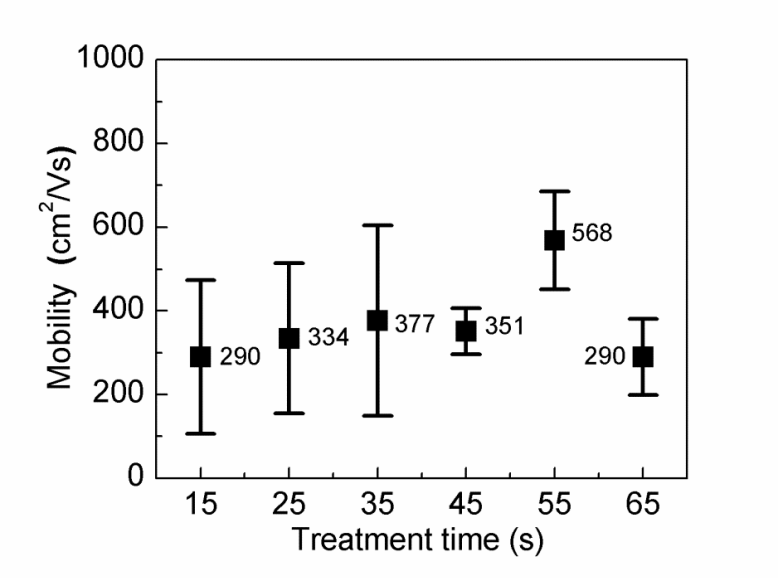

Figure S10 Mobility versus treatment time. The error bar width shows the mobility range with a tight distribution. The mobility was enhanced by our new processing.

Figure S11

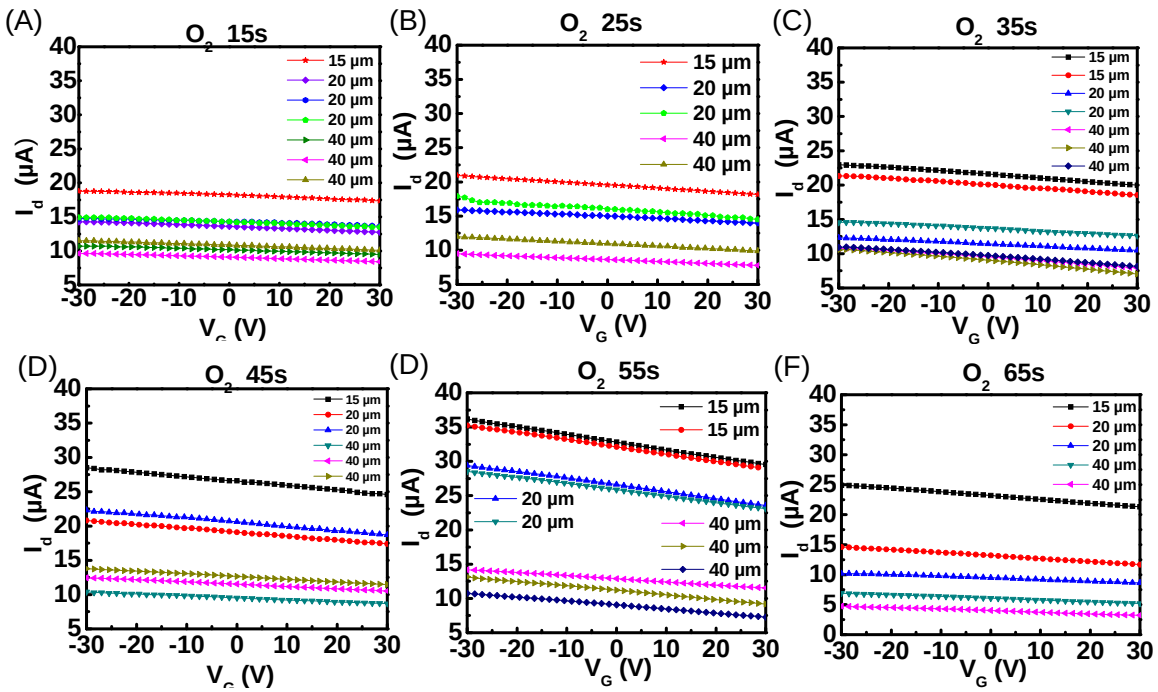

Figure S11. Transfer characteristics of the devices. Six sets of devices were processed under 15, 25, 35, 45, 55, and 65s plasma treatments. Here, we show the carrier transport characteristics of the back-gating FET having L_{ch} = 15μm, 20μm, and 40μm. The figures show the enhancement of carrier transport at room-temperature (mobility).

3. Electrical properties of the devices fabricated by O_2 pre-plasma processing for 5s.

Figure S12

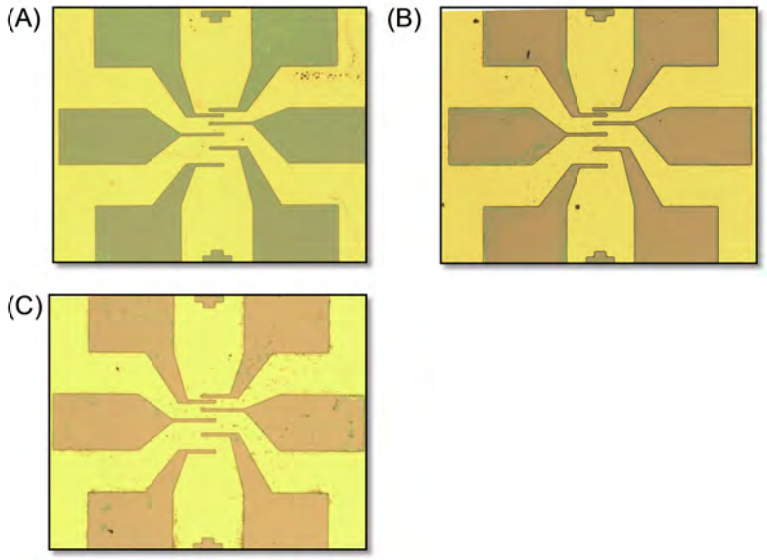

Figure S12. (A) OM images of the sample with TLM pattern after photolithography. The dark blue area was covered with pristine graphene. (B) Sample after O_2 plasma for 5s treatment. It can be clearly seen that graphene area changed which is distinguished from the colour. But it still remained a film, which means no etching occurred. (C) Sample after O_2 plasma for 45s treatment makes clearly comparison to 5s treatment sample.

Figure S13

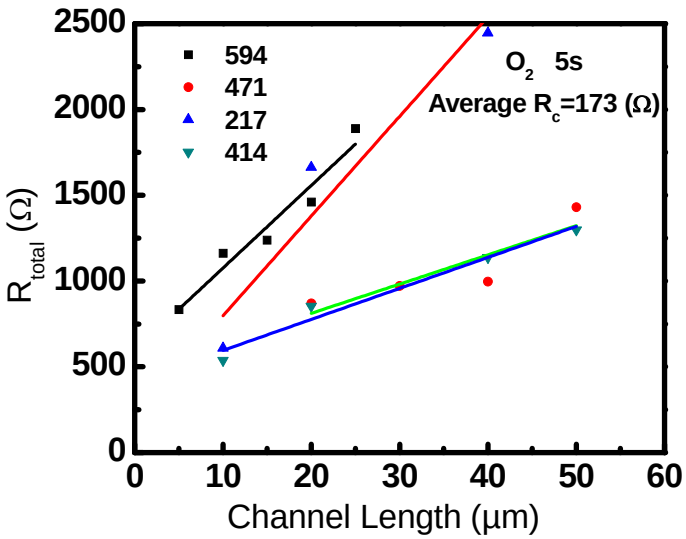

Figure S13. Derivation of contact resistance (R_c) using TLM at a gate biase of 0.01V for the sample after 5s plasma treatment. The average R_c is 173Ω.

4. Raman data to ensure that the quality of graphene is comparable and selected graphene regions are consistent prior to plasma treatment.

Figure S14

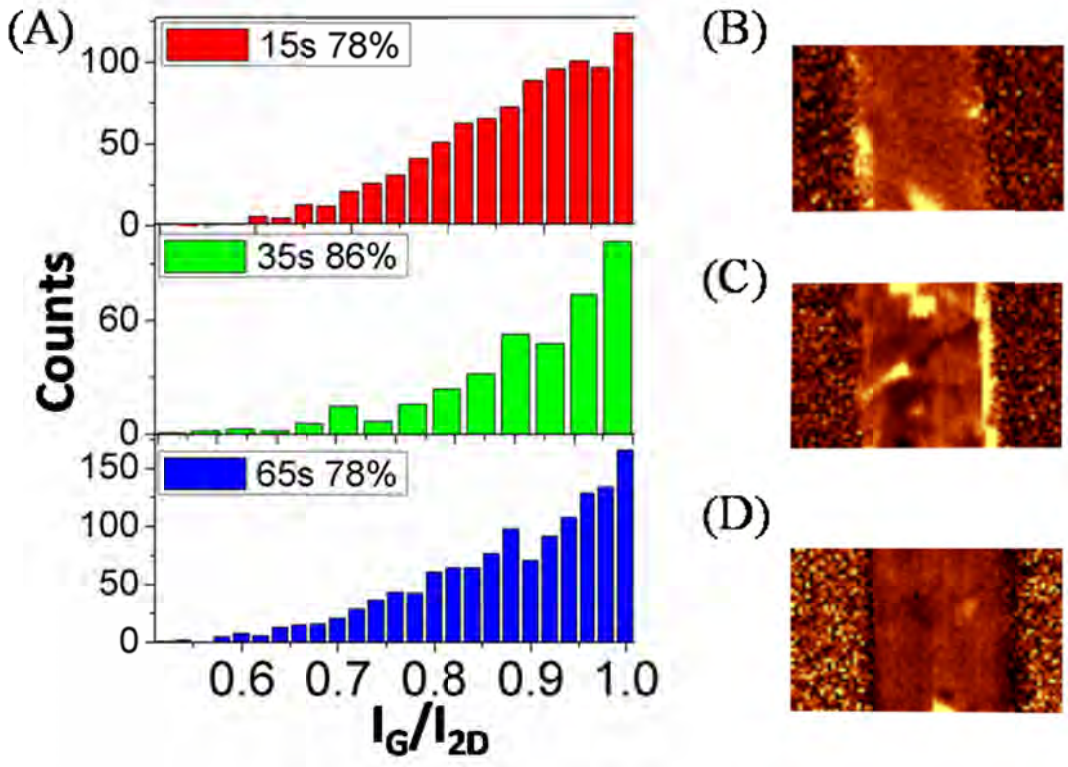

Figure S14 (A) Statistical histograms for I_G/I_{2D} ratio. (B)-(D) The corresponding Raman mapping images of I_G/I_{2D} ratio.

5. SEM data to reveal the effects of pre-plasma treatment on the edge structure of PR.

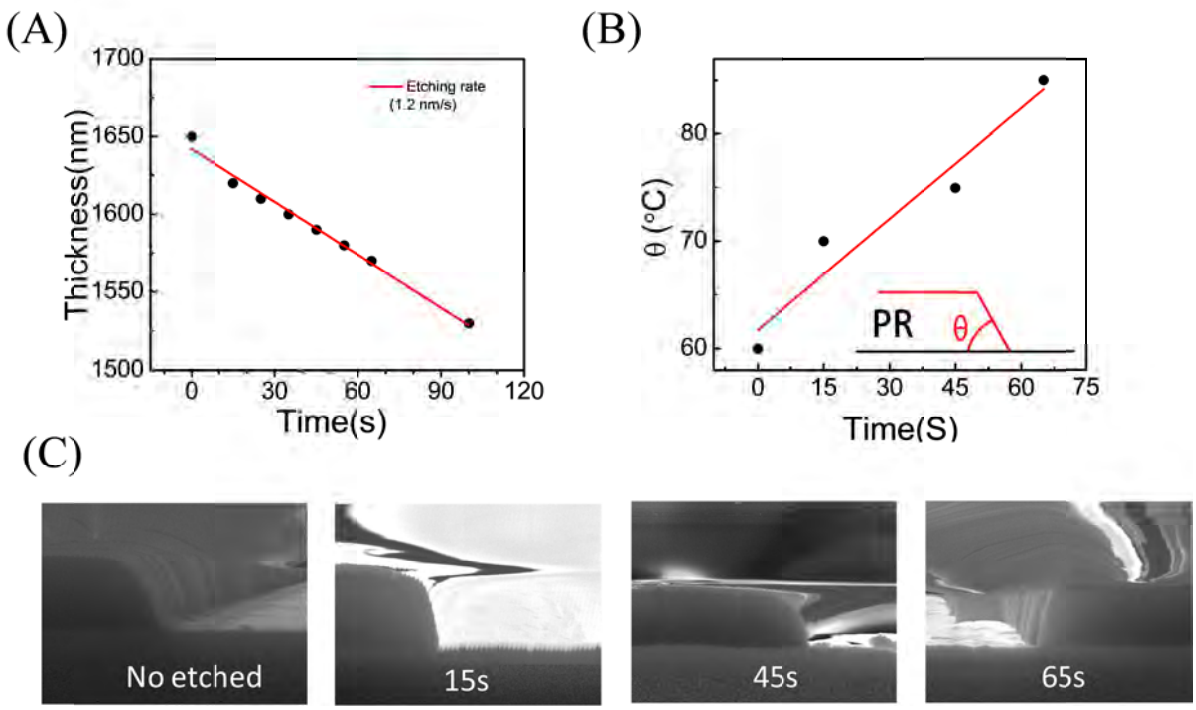

Figure S15. Effects of plasma treatment on the edge structure of PR. (A) Thickness of PR vs. plasma treatment time. (B) Angle of developed PR. (C) SEM images of the PR films before etching and after the treatment for three controlled plasma processing times of 15, 45, and 65s. Variation at the edge of PR is observed.

6. References

1. K. Nagashio, T. Nishimura, K. Kita and A. Toriumi, Electron Devices Meeting (IEDM), 2009 IEEE International, 2009.
2. S. Russo, M. Craciun, M. Yamamoto, A. Morpurgo and S. Tarucha, *Physica E: Low-dimensional Systems and Nanostructures*, 2010, 42, 677-679.
3. L. Wang, I. Meric, P. Y. Huang, Q. Gao, Y. Gao, H. Tran, T. Taniguchi, K. Watanabe, L. M. Campos, D. A. Muller, J. Guo, P. Kim, J. Hone, K. L. Shepard and C. R. Dean, *Science*, 2013, 342, 614-617.
4. W. S. Leong, H. Gong and J. T. Thong, *ACS nano*, 2013, 8, 994-1001.
5. T. Chu and Z. Chen, *ACS nano*, 2014, 8, 3584-3589.
6. A. D. Franklin, S.-J. Han, A. A. Bol and V. Perebeinos, *Electron Device Letters, IEEE*, 2012, 33, 17-19.
7. J. T. Smith, A. D. Franklin, D. B. Farmer and C. D. Dimitrakopoulos, *ACS nano*, 2013, 7, 3661-3667.
8. A. Hsu, H. Wang, K. K. Kim, J. Kong and T. Palacios, *Electron Device Letters, IEEE*, 2011, 32, 1008-1010.
9. F. Xia, V. Perebeinos, Y.-m. Lin, Y. Wu and P. Avouris, *Nature nanotechnology*, 2011, **6**, 179-184.
10. M. S. Choi, S. H. Lee and W. J. Yoo, *Journal of Applied Physics*, 2011, **110**, 073305.